ACS Catalysis

Research Article

pubs.acs.org/acscatalysis

Bioinspired Silica Nanocomposite with Autoencapsulated Carbonic Anhydrase as a Robust Biocatalyst for CO_2 Sequestration

Byung Hoon Jo,[†,‡] Jeong Hyun Seo,[‡,§] Yun Jung Yang,[‡] Kyungjoon Baek,[∥] Yoo Seong Choi,[⊥] Seung Pil Pack,[#] Sang Ho Oh,[∥] and Hyung Joon Cha*[,†,‡]

[†]School of Interdisciplinary Bioscience and Bioengineering, Pohang University of Science and Technology, Pohang 790-784, Korea

[‡]Department of Chemical Engineering, Pohang University of Science and Technology, Pohang 790-784, Korea

[§]School of Chemical Engineering, Yeungnam University, Gyeongsan 712-749, Korea

[∥]Department of Materials Science and Engineering, Pohang University of Science and Technology, Pohang 790-784, Korea

[⊥]Department of Chemical Engineering, Chungnam National University, Daejeon 305-764, Korea

[#]Department of Biotechnology and Bioinformatics, Korea University, Sejong 339-700, Korea

ABSTRACT: Here, we report on the development and characterization of a carbonic anhydrase (CA)-based biocatalyst encapsulated in a biosilica matrix for use in environmental CO_2 sequestration. Encapsulation occurred simultaneously with autonomous silica synthesis by silica-condensing R5 peptide that was fused to recombinant CA. The encapsulation efficiency was greater than 95%, and the encapsulated CA was not leached from the silica matrix, demonstrating the highly efficient R5-mediated autoencapsulation process. The catalytic efficiencies for both esterase and CO_2 hydratase activities tended to increase with increasing pH; however, the catalytic efficiency for CO_2 hydration was much more pH dependent, suggesting that proton transfer from silica to water is a rate limiting step, especially for CO_2 hydration. In addition to good reusability, the encapsulated CA exhibited outstanding thermostability, even retaining 80% activity after 5 days at 50 °C. The thermoactivity was also remarkable, showing ~10-fold higher activity at 60 °C compared to that at 25 °C. The physical structure was observed to be highly compact with a low surface area, stressing the importance of the outermost surface for catalytic performance. We also demonstrated the applicability of the silica nanoparticle to the sequestration of CO_2 in carbonate minerals. The rate of $CaCO_3$ precipitation was remarkably accelerated by the encapsulated biocatalyst. The biosilica nanocomposite exhibited ~60% of the CO_2 sequestrating power of the free enzyme, which is expected to be the maximal ability of the encapsulated CA. Thus, this silica-CA nanocomposite, efficiently synthesized via a biomimetic green route, can be successfully used as a robust biocatalyst for biomimetic sequestration of the greenhouse gas CO_2.

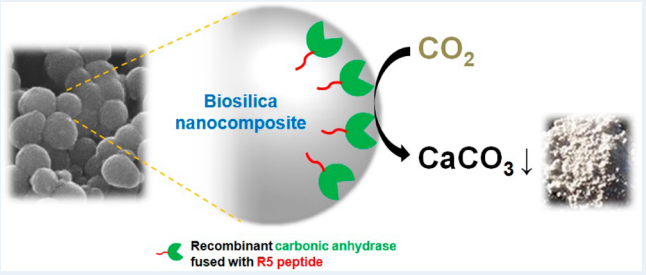

KEYWORDS: *CO_2 sequestration, carbonic anhydrase, immobilization, biomineralization, silaffin, biosilica*

1. INTRODUCTION

Reduction of the major greenhouse gas, carbon dioxide (CO_2), has been regarded as one of the most urgent issues for sustainable environment. Although traditional methods for CO_2 capture, including chemical absorption and physical separation, have been demonstrated to be effective, they have some limitations, such as high cost and generation of pollutants.[1] Novel methods or materials for reduction of CO_2 have been proposed,[2] among which biomimetic CO_2 capture, employing the enzyme carbonic anhydrase (CA), is considered to be one of the most promising approaches because of the green nature of enzyme-based methods and the anticipated cost reduction.[3,4]

CA is a zinc metalloenzyme that rapidly catalyzes the hydration of CO_2, with the concomitant generation of bicarbonate and a proton, which is one of the rate limiting steps in CO_2 sequestration in aqueous solutions.[5] Despite the enzyme's remarkably fast rate of catalysis, its application is strongly limited by its low stability and poor reusability,[6] issues that are commonly encountered in enzyme applications. These problems have been partially circumvented by immobilizing CA onto various support materials such as silica,[7] glass,[8] polyurethane foam,[9] and chitosan,[10] in which CAs were endowed with enhanced thermostability and improved recovery of enzyme. However, all of the methods employed require harsh conditions and extended periods of time for either material preparation or enzyme immobilization, generally resulting in low immobilization efficiency and severe reduction of enzymatic activity.

Biochemical and genetic studies on biosilica formation in marine diatoms and sponges led to the discovery of the involvement of organic components such as proteins and amines in the in vivo biosilicification.[11] These organics were demonstrated to rapidly promote in vitro sol−gel silica

Received: June 16, 2014
Revised: September 19, 2014
Published: October 16, 2014

   dx.doi.org/10.1021/cs5008409 | ACS Catal. 2014, 4, 4332−4340

polycondensation and precipitation under ambient conditions (at neutral pH and room temperature), and this remarkable ability has been applied mainly to simultaneous encapsulation of protein during the synthesis of silica nanocomposites for the development of efficient catalysts or sensors.[12] Recently, it was reported that CA encapsulated in silica nanoparticles via an amine-based method exhibited high immobilization efficiency, enhanced stability and reusability. Furthermore, the facile, rapid, and mild encapsulation process permitted a high level of activity retention after immobilization of the enzyme.[3] However, it also revealed some defects, including a low amount of enzyme loading in a single reaction and considerable enzyme leakage that can limit long-term industrial use of the catalyst. Thus, more efficient routes are required for CA encapsulation in biosilica to ensure high performance in CO_2 sequestration.

Silaffins are highly post-translationally modified proteins found in silica cell walls of the diatom *Cylindrotheca fusiformis*.[13] One of the repeating units of a silaffin protein, R5 peptide (H_2N-SSKKSGSYSGSKGSKRRIL-COOH), was shown to induce rapid precipitation of silica, even without post-translational modifications,[13] and thus has been used as an effective additive for bioinspired enzyme encapsulation under ambient conditions.[12,14,15] A clever technique is the construction of translational fusion enzymes with R5 that have been demonstrated to be functional in both enzymatic activity and silica polycondensation and can then facilitate autoencapsulation of the enzymes.[16] When fused with R5 peptide, each enzyme molecule would be conferred with the abilities of both silica synthesis and binding, which could maximize homogeneous enzyme loading in a one-pot reaction and minimize enzyme leakage. It would also facilitate the preparation of materials because there would be no need for synthesis of R5 peptide separately from enzyme production.

In the present work, CA from *Neiserria gonorrhoeae* (*ng*CA), one of the fastest CAs known, with a turnover number of $\sim 10^6$ s^{-1},[17] was genetically fused with R5 peptide. Recently, we reported the functional overexpression of recombinant *ng*CA in *Escherichia coli* and the subsequent application of this enzyme to CO_2 sequestration.[5,18] Here, we demonstrate that a silica-CA nanocomposite, synthesized via R5-mediated autoencapsulation, is a robust, green biocatalyst for CO_2 sequestration.

2. MATERIALS AND METHODS

2.1. Bacterial Strains and Vector Construction. All DNA work was performed using *E. coli* TOP10 (Invitrogen, USA) following standard protocols. *E. coli* BL21 (DE3) (Novagen, USA) was used as a host strain for fusion protein expression. The *ng*CA gene, as a secretion signal-truncated form, was polymerase chain reaction (PCR)-amplified from *N. gonorrhoeae* genome using the primers (forward 5′-CATATG-CACGGCAATCACA-3′ and reverse 5′-AAGCTTTTCA-ATAACTACACGTGCATTC-3′; the underlined are restriction sites for *Nde*I and *Hind*III, respectively). The PCR product was ligated into pGEM T-easy (Promega, USA), and the gene sequence was verified by direct sequencing. The *ng*CA gene was liberated by digestion of the vector with *Nde*I and *Hind*III and was subcloned into pET-22b(+) vector (Novagen) treated with the same endonucleases, resulting in pET-ngCA. The synthetic complementary primers (forward 5′-AGCT*TAGCAG-CAAAAAATCTGGCTCCTATTCAGGCTCGAAAGGTT-CTAAACGTCGCATTCTGC*-3′ and reverse 5′-TCGA-*GCAGAATGCGACGTTTAGAACCTTTCGAGCCTGAATAG-GAGCCAGATTTTTTGCTGCTA*-3′; the underlined are single-stranded overhangs from *Hind*III and *Xho*I digestion, respectively) containing R5 peptide sequence (italic) were annealed and ligated into a pET-ngCA vector treated with *Hind*III and *Xho*I, resulting in pET-ngCA:R5. The fusion DNA construct was also confirmed by direct sequencing. The final vector has a hexahistidine (His_6)-tag sequence at its *C*-terminus.

2.2. Preparation of Recombinant *ng*CA-R5 Fusion Protein. *E. coli* BL21 (DE3) was transformed with pET-ngCA or pET-ngCA:R5 and grown at 37 °C in Luria−Bertani (LB) medium (Usb Corp., USA) supplemented with 50 μg/mL ampicillin (Sigma-Aldrich, USA). Expression of the recombinant protein was induced at mid log growth phase by adding 1 mM isopropyl-β-D-thiogalactopyranoside (IPTG; Carbosynth, UK) and 0.1 mM $ZnSO_4$ (Sigma-Aldrich) to the medium. Cell growth along with protein expression continued for 6−8 h, and the cells were then harvested by centrifugation at 4 °C and 4000 × *g* for 10 min. The harvested cells were washed and resuspended in lysis buffer (20 mM Tris-sulfate, 300 mM NaCl, and 10 mM imidazole; pH 8.3). The cells were lysed using an ultrasonic dismembrator (Sonics and Materials, USA) for 20 min at 20% amplitude (3 s pulse on and 12 s pulse off) on ice. After centrifugation at 4 °C and 10 000 × *g* for 20 min, the supernatant was removed and designated as the soluble fraction. The remaining pellet was designated as the insoluble fraction. The soluble fraction was used for enzyme purification by affinity chromatography using Ni-nitrilotriacetic acid (NTA) agarose beads (Qiagen, USA) according to the manufacturer's instructions. The eluted enzyme was dialyzed against Tris-sulfate buffer (20 mM; pH 8.3 at 25 °C) at 4 °C. The dialyzed enzyme solution was concentrated using an ultrafiltration membrane (Millipore, USA), which was designated enzyme stock solution.

2.3. SDS-PAGE and Western Blot Analyses. Protein samples were separated by sodium dodecyl sulfate-polyacrylamide gel electrophoresis (SDS-PAGE), and the gel was stained with Coomassie Brilliant Blue G-250 (Bio-Rad, USA). For Western blots, proteins on the gel were blotted onto a nitrocellulose membrane (Whatman, USA), and the membrane was subjected to sequential treatments of primary antibody (monoclonal anti-His_6 antibody; ABM, Canada) and secondary antibody (alkaline phosphatase-conjugated antimouse IgG; Sigma-Aldrich). The recombinant *ng*CA proteins were detected with nitro blue tetrazolium/5-bromo-4-chloro-3-indolyl phosphate (NBT/BCIP; Sigma-Aldrich).

2.4. Enzyme Encapsulation. Enzyme was encapsulated during silica deposition as previously described[14,16] with slight modifications. Tetramethyl orthosilicate (TMOS; Sigma-Aldrich, 1 M final concentration), a precursor of silicic acid, was acid-hydrolyzed for 30 min in 1 mM hydrochloric acid. Silica was precipitated by mixing 900 μL of the enzyme stock solution (enzyme in 20 mM Tris-sulfate, pH 8.3) with 100 μL of the prehydrolyzed 1 M TMOS (pH 2.7), which resulted in reaction solution with pH 7.8. If necessary, the total volume was changed, but the volume ratio was always kept to be 9:1. After 5 min, the resultant silica was separated by centrifugation for 5 min at 10 000 × *g*. The supernatant was removed and stored for measuring the unencapsulated amount of enzyme. The pellet was washed twice with deionized water (DW) by repeated resuspension and centrifugation, and each supernatant after washing was also stored for further analysis. The washed silica was finally resuspended in the same volume of DW. All reactions were performed at room temperature. To examine

dx.doi.org/10.1021/cs5008409 | ACS Catal. 2014, 4, 4332−4340

encapsulation efficiencies at different enzyme concentrations, enzyme encapsulation was performed using enzyme stock solutions that were diluted with Tris-sulfate buffer (20 mM, pH 8.3) to appropriate enzyme concentrations (0.5−10 mg/mL).

2.5. Protein Quantification. The concentration of purified protein was measured using the Bradford reagent (Bio-Rad), with bovine serum albumin (BSA; Sigma-Aldrich) as a standard. Because both Tris buffer and hydrolyzed TMOS solution reacted with the Bradford reagent and slightly interfered with the quantification, the initially measured protein concentration was correlated with absorbance at 280 nm, which was used for measuring protein concentration throughout the experiments (data not shown). Neither Tris nor hydrolyzed TMOS absorbed light at 280 nm.

2.6. Enzyme Leakage Test. Immediately after silica synthesis and washing, the silica resuspended in DW was stored at 4 °C. At the indicated time points, the particles were centrifuged at 4 °C and 10 000 × *g* for 20 min. After the protein content of the supernatant was measured at 280 nm, the supernatant was restored back to the silica pellet, which was then resuspended and further stored.

2.7. CA Activity Assay. Enzyme activity was determined by assaying for both esterase activity (hydrolysis of *p*-nitrophenyl acetate (*p*-NPA; Sigma-Aldrich)) and CO_2 hydration. For the esterase assay, 200 μL (50 μL for pH 9.0) of 30 mM *p*-NPA (3 mM (0.75 mM for pH 9.0) final concentration) dissolved in acetonitrile was introduced into a reaction mixture consisting of 1.7 mL (1.9 mL for pH 9.0) of 50 mM potassium phosphate buffer (pH 6.0, 7.0, or 9.0) and 100 μL (50 μL for pH 9.0) of enzyme (or silica). After reaction with gentle stirring at 25 °C, the absorbance at 405 nm (the absorption maximum of *p*-nitrophenolate, the product of *p*-NPA hydrolysis) or at 348 nm (the isosbestic point of *p*-nitrophenolate and *p*-nitrophenol; for pH 6.0) was measured. The pH was almost retained during the reaction. For each test sample, two separate reactions were performed; one was immediately measured after mixing the reactants, and the other was measured after 10 min (30 min for pH 6.0) of reaction. The absorbance difference was used for calculation of the relative hydrolysis rate. For silica samples, the reaction mixtures were centrifuged for 1 min at 10 000 × *g* before the absorbance measurement of the supernatant. For a set of tests, a blank experiment was conducted to measure the self-dissociation rate of *p*-NPA by adding an appropriate amount of phosphate buffer instead of enzyme, and the resulting rate was subtracted from the rates of other samples.

For the measurement of CO_2 hydration activity, a stopped-flow spectrometer (Applied Photophysics, UK) was used along with a colorimetric method.[17] The buffer/indicator systems were 2-(N-morpholino)ethanesulfonic acid (MES)/NaOH with chlorophenol red (pH 6.2) measured at 572 nm, 3-(*N*-morpholino)propanesulfonic acid (MOPS)/NaOH with *p*-nitrophenol (pH 7.3) measured at 405 nm, and *N*-Tris-(hydroxymethyl)methyl-3-aminopropanesulfonic acid (TAPS)/NaOH with *m*-cresol purple (pH 8.5) monitored at 578 nm. Activities above pH 8.5 could not be tested due to the lack of an available buffer/indicator pair. The buffer concentrations were 50 mM for MES and 100 mM for both MOPS and TAPS. The ionic strength was maintained at ∼0.1 M using Na_2SO_4. The indicators were used at a concentration of 486 μM for *p*-nitrophenol and 97.2 μM for the others. Buffers containing predissolved enzyme (or silica) were mixed with the same volume of CO_2-saturated water inside the stopped-flow cell, and the absorbance changes were recorded at each wavelength. Blank experiments (uncatalyzed reactions) were also conducted. The initial rates obtained were used for the calculation of relative rates. All preparations and reactions were performed at 25 °C.

2.8. Reusability. Reusability of the CA-encapsulated silica nanoparticles was tested using esterase activity assay with slight modifications. To minimize loss of silica and/or decrease of activity due to adsorption of silica to plasticwares, specialized pipet tips (Gene Era Biotech, USA) and a glass tube (Takara, Japan) were used. To initiate enzymatic reaction, 100 μL of 30 mM *p*-NPA was added into a reaction mixture containing 300 μL of silica and 600 μL of 50 mM potassium phosphate buffer (pH 7.0). After 5 min at 25 °C, the reaction tube was centrifuged for 1 min at 9000 × *g* and the absorbance of supernatant was measured at 405 nm. The silica was washed with DW and resuspended in 300 μL of DW, which was then reused for the next assay in the same way.

2.9. Thermostability and Thermoactivity. For thermostability test, enzyme and silica solutions were incubated at the indicated temperatures inside a heating oven. Samples were then stored at 4 °C until the activities were measured. Activities were estimated using *p*-NPA at pH 7.0 and 25 °C as previously described, and the residual activities were calculated based on the activities of the untreated (originally store at 4 °C) samples as follows.

$$\text{residual activity (\%)} = \frac{\text{activity of heat treated sample}}{\text{activity of untreated sample}} \times 100$$

Thermoactivity was evaluated by measuring enzyme activities using *p*-NPA at various temperatures (25−70 °C). One hundred microliters of enzyme (or silica) solution was added into 1.85 mL of 50 mM potassium phosphate buffer (pH 7.0) preincubated at each temperature. Fifty microliters of 30 mM *p*-NPA (0.75 mM final concentration) was then immediately mixed, and the absorbance at 348 nm was measured after 5 min reaction. Blank experiment was also conducted at each temperature, with which all the results were corrected to obtain enzymatic reaction rates.

2.10. Measurements of Particle Size Distribution, ζ Potential, and Surface Area. Particle size distribution and surface charge of the silica nanoparticles were measured and analyzed with a Zetasizer (Malvern Instruments, UK) at 25 °C. Surface area was estimated by the Brunauer−Emmett−Teller (BET) method from the linear monolayer region of adsorption in N_2 isotherms performed on an ASAP 2010 (Micromeritcs, USA) at −196 °C. Pore volume was calculated using the Barrett−Joynes−Halenda (BJH) method.

2.11. Electron Microscopy Analyses. For scanning electron microscopy (SEM), samples were dried at 70 °C overnight and analyzed on a JSM-6010LV (JEOL, Japan). Silica samples for transmission electron microscopy (TEM) were dispersed in ethanol, and the suspension was placed on a carbon-coated copper grid and dried for 1 h in a vacuum oven before analysis. Analyses of selected area electron diffraction (SAED) patterns and high-resolution TEM, as well as conventional diffraction contrast TEM in bright-field mode, were performed on a JEM-2100F (JEOL) operated at 200 kV.

2.12. CO_2 Sequestration in $CaCO_3$. Free enzyme was diluted to 0.60 mg/mL (1.0 ×), 0.42 mg/mL (0.7 ×), 0.36 mg/mL (0.6 ×), and 0.30 mg/mL (0.5 ×) using Tris-sulfate buffer (20 mM; pH 8.3). Silica sample was similarly diluted

dx.doi.org/10.1021/cs5008409 | ACS Catal. 2014, 4, 4332−4340

using DW to have the same protein content as the 1.0× free enzyme. The sequestration of CO_2 in $CaCO_3$ was performed as previously described with slight modifications.[5] CO_2-saturated water (500 μL, prepared at 30 °C) was added to a reaction cuvette containing 450 μL of buffer (1 M Tris and 20 mM $CaCl_2$; pH 11) and 50 μL of the prepared sample (or DW as blank). $CaCO_3$ precipitation was performed at 30 °C and turbidimetrically monitored at 600 nm using a UV/vis spectrophotometer (Shimadzu, Japan). The time required for onset of precipitation (defined as the first second of the time period that showed an average rate of increase more than 0.001 A_{600}/s) was recorded. The resulting absorbance curves were also examined to compare the initial precipitation rates after the onset of precipitation. The final pH value of buffer was approximately 9.3.

For characterization of $CaCO_3$, CO_2 was mineralized in a 40 mL-reaction mixture instead of 1 mL in order to obtain a sufficient amount of the carbonate mineral. After 5 min, the mixture was filtered through a 0.45 μm membrane filter (Millipore, USA). The precipitates that were on the membranes were dried at 70 °C overnight. Identities and polymorphs of the precipitates were analyzed by X-ray powder diffraction (XRD) and SEM as previously described.[5]

3. RESULTS AND DISCUSSION

3.1. Encapsulation of *ng*CA-R5 Fusion Protein in Silica Nanoparticles. The R5 peptide sequence was genetically tethered to the C-terminus of *ng*CA gene with His_6-tag provided by the parent vector, as shown in Figure 1a. This

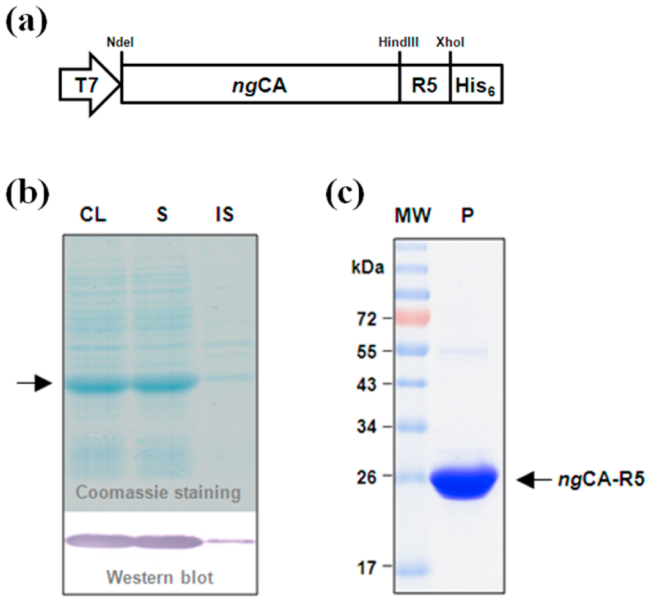

Figure 1. (a) Gene construction, (b) expression, and (c) purification of *ng*CA-R5 fusion protein. Lanes for SDS-PAGE and Western blot: CL, cell lysate; S, soluble fraction; IS, insoluble fraction; MW, molecular weight markers; P, purified protein.

produced a fusion protein with a theoretical molecular weight of 28.75 kDa, which was highly overexpressed as a soluble form in *E. coli* (Figure 1b). The recombinant fusion enzyme, *ng*CA-R5, was purified to homogeneity using His_6-tag metal affinity chromatography, with a final yield of ~0.1 g soluble protein per liter of culture (Figure 1c).

When hydrolyzed TMOS was added to *ng*CA-R5 solution under ambient conditions, the formation of white silica precipitates (*ng*CA-R5@silica) was apparent within several seconds, while the same buffer solution containing *ng*CA without R5 did not exhibit silica formation (Figure 2a),

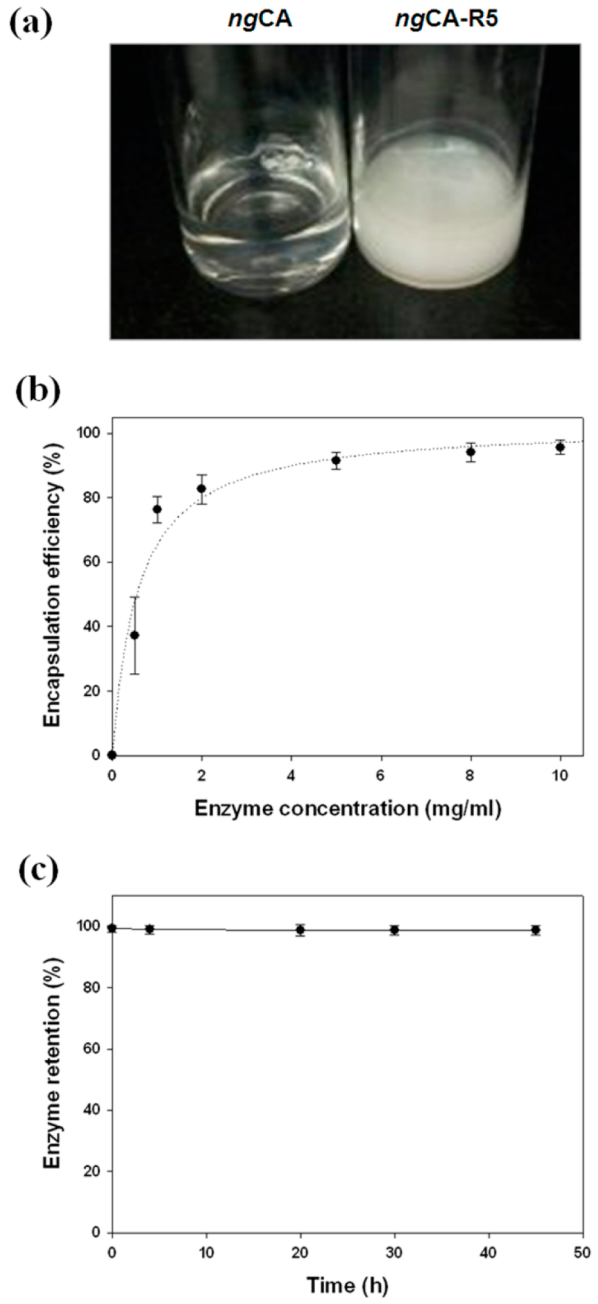

Figure 2. (a) Silica formation by *ng*CA without R5 (left) and *ng*CA-R5 (right). (b) CA encapsulation efficiency at various enzyme concentrations. (c) Enzyme leaching according to incubation time.

indicating that the 19 amino acid-length R5 peptide is crucial for the synthesis of silica. To optimize enzyme encapsulation efficiency, the concentration of enzyme stock solution was varied from 0.5 to 10 mg/mL. The results demonstrate that higher ratios of enzymes can be immobilized in the silica matrix when higher concentrations of enzymes are present in the reaction solution (Figure 2b). Approximately 90% of the enzymes were encapsulated using a 5 mg/mL stock solution,

dx.doi.org/10.1021/cs5008409 | ACS Catal. 2014, 4, 4332−4340

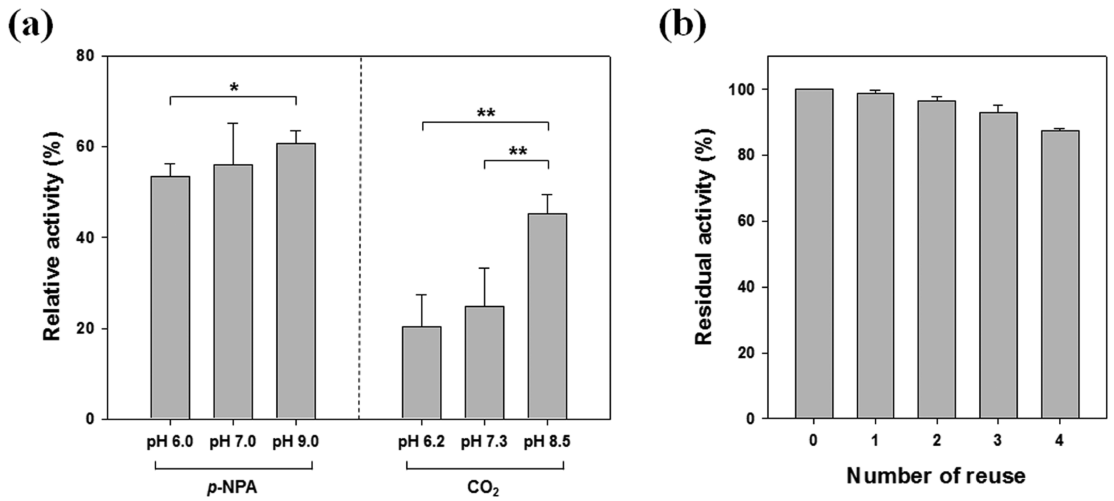

Figure 3. (a) Retention of enzyme activity after silica encapsulation assayed by *p*-NPA hydrolysis and CO_2 hydration assays under various pH conditions. The asterisks indicate differences with statistical significance (*$p < 0.05$, **$p < 0.01$, one-way ANOVA). (b) Reusability of *ng*CA-R5@silica.

and the efficiency was increased to greater than 95% when 10 mg/mL was used. Accordingly, all the subsequent experiments were performed with 10 mg/mL enzyme stock solutions. The relation between the enzyme concentration and the encapsulation efficiency (not the amount of encapsulated enzyme) showed a hyperbolic curve, most likely implying the involvement of the enzyme in the silica-forming reaction as both a reactant and a catalyst (its R5 moiety). It was reported that the use of amines as a silica-forming additive led to high encapsulation efficiency only when the concentration of enzyme was relatively low, and the efficiency was reduced to ~40% with the addition of 10 mg CA.[3] Thus, increased enzyme loading with increased enzyme concentration seems to be a unique feature of self-encapsulation of protein onto biosilica mediated by the fused R5 peptide.

It is desirable that once immobilized, enzyme should be retained in the matrix so that no leaching occurs from the solid support. Obviously, this is a more important issue than the encapsulation process itself in a long-term industrial application of the immobilized biocatalyst. We tested enzyme leaching by measuring protein content of the supernatant in the silica suspension after thorough centrifugation, and found that the autoencapsulated enzyme was strongly entrapped inside the silica (Figure 2c). During the initial washes, the fraction of desorbed proteins was below 1% of the total encapsulated enzymes. When the washed silica particles were stored for 45 h, less than 0.5% of the initial enzyme content leached from the support. Because the absorbance of the supernatant was virtually maintained throughout the measurements from 4 to 45 h, the apparent leaching of 0.5% is likely because of trace amounts of silica particles that were incidentally included in the measurement that could affect the absorbance at 280 nm. Therefore, we concluded that the autoencapsulation is an extremely effective method showing negligible enzyme leakage, while the amine-based biosilica lost ~10% of the enzyme during 24 h of storage.[3] Silaffins were found to be tightly bound to silica even after boiling with SDS, which is a strong detergent for protein solubilization.[13] The R5 peptide, even without any post-translational modifications, also seems to tightly bind to silica after silica synthesis. The enzyme covalently linked to the R5 moiety directly benefits from this strong interaction, resulting in efficient retention of the encapsulated enzyme.

3.2. Enzymatic Performance of *ng*CA-R5@silica. The enzymatic activity of encapsulated CA was compared with its free enzyme counterpart by measuring the activities for both *p*-NPA hydrolysis and CO_2 hydration, reactions that can be catalyzed by the same active site of CA.[19] To exactly probe the extent of activity reduction when an enzyme is immobilized, we considered the dilution factor (9:1 ratio of enzyme solution to hydrolyzed TMOS), encapsulation efficiency, and enzyme leaching during washing in the calculation and comparison of the activities. The *ng*CA-R5@silica retained ~53−60% of the free enzyme activity for *p*-NPA hydrolysis (Figure 3a), which is comparable to that of CA encapsulation in amine-based biosilicas.[3] This performance exceeds those of CA-assisted, biomineralized calcium carbonate crystalline composites (~43%)[20] and traditional immobilization of CA on glass (~38%).[8] In contrast, interestingly, only 20% of free enzyme activity for CO_2 hydration was retained in the encapsulated CA at relatively low pH (6.2), and was observed to increase, depending on the pH, retaining 45% at pH 8.5 (Figure 3a).

The catalytic cycle of CA consists of two steps,[21] the interconversion between CO_2 and HCO_3^- (eq 1a) and the regeneration of the active site by intramolecular (eq 1b) and intermolecular (eq 1c) proton transfers as follows:

$$\mathrm{PSR{-}E{-}Zn^{2+}{-}OH^- + CO_2 + H_2O \leftrightarrow PSR{-}E{-}Zn^{2+}{-}H_2O + HCO_3^-} \quad (1a)$$

$$\mathrm{PSR{-}E{-}Zn^{2+}{-}H_2O \leftrightarrow H^+{-}PSR{-}E{-}Zn^{2+}{-}OH^-} \quad (1b)$$

$$\mathrm{H^+{-}PSR{-}E{-}Zn^{2+}{-}OH^- + B \leftrightarrow PSR{-}E{-}Zn^{2+}{-}OH^- + BH^+} \quad (1c)$$

(where E = enzyme, PSR = proton shuttle residue, and B = external buffer).

Because biosilica itself has the capability of proton buffering,[22] an additional proton pathway via silica can be described.

dx.doi.org/10.1021/cs5008409 | ACS Catal. 2014, 4, 4332−4340

$$H^+—PSR—E—Zn^{2+}—OH^- + S \leftrightarrow PSR—E—Zn^{2+}—OH^- + SH^+ \quad (1d)$$

$$SH^+ + B \leftrightarrow S + BH^+ \quad (1e)$$

(where S = silica).

Since proton transfer is the rate-limiting step of the catalytic cycle of CO_2 hydration in free CA,[21] relative enzymatic rate of encapsulated CA compared to free enzyme can be lowered if proton transfer is further limited by enzyme-encapsulating material. Therefore, the strong pH dependence of CO_2 hydration shown in Figure 3a suggests that proton transfer from PSR to buffer (and instantaneously to water) via silica (eq 1d and 1e) is the major limiting step. This is also supported by the surface charge of *ng*CA-R5@silica; it is more negatively charged at higher pH, thereby allowing facilitated proton transfer (Table 1). Note that this pH dependence of the *relative* activity of encapsulated CA to free form of enzyme is distinct from the pH dependence of the *absolute* activity of CA itself, which is much higher at higher pH regardless of the substrates.[17]

Table 1. Surface Characteristics of *ng*CA-R5@silica[a]

ζ-potential (mV)					
pH 6.2	pH 7.3	pH 8.5	S_{BET} (m^2/g)	V (cm^3/g)	D (Å)
−0.3	−4.7	−7.0	7.68	0.00197	10.2

[a]Abbreviations: S_{BET}, BET surface area; V, total pore volume; d, average pore diameter.

Although studies on proton transfer in CA have been conducted using CO_2 as the primary substrate, some data from studies on catalytic activities of site-specific CA mutants suggest that proton transfer is also the rate-limiting step of *p*-NPA hydrolysis.[23,24] While the catalysis of CO_2 hydration by CA is extremely fast (10^4−10^6 s^{-1}), esterase activity of CA is generally very slow (<10 s^{-1}).[17,25] The weak pH dependence of esterase activity (Figure 3a) can be explained by this slow activity, in that silica is capable of dealing with a small amount of protons generated from encapsulated CA without significant delay throughout the range of pH values. Thus, the lowered catalysis itself by encapsulation and/or the substrate diffusion, rather than the product transfer, may be the major limiting factors in *p*-NPA hydrolysis. Accordingly, the relative activity of approximately 60% seems to be the upper limit that can be obtained by encapsulated CA in silica nanoparticles compared with the free form of the enzyme.

Next, we examined the activity retention of the encapsulated CA after repeated reuses to assess reusability. It was shown that *ng*CA-R5@silica retained 99% and 87% of the initial activity when reused once and four times, respectively, in *p*-NPA hydrolysis assay (Figure 3b). This fairly good reusability can be attributed to the strong retention (Figure 2c) and the stabilization (see Section 3.3 below) of the encapsulated enzyme in silica matrix. The slight, but gradual decrease of residual activity after each reuse cycle seems to result mainly from decreased activity by adsorption of silica to the reaction tube during centrifugation and/or by incidental loss of silica particles during removal of supernatant after centrifugation, not by decrease of activity per each silica particle itself. Thus, *ng*CA-R5@silica is a robust catalyst that can be easily recycled for potential industrial usage without severe loss of activity.

3.3. Thermostability and Thermoactivity of *ng*CA-R5@silica. In general, enzyme stabilization is the most prominent effect of immobilization. The thermostability of *ng*CA-R5@silica was assessed by measuring *p*-NPA hydrolysis activity at 25 °C after incubating the catalyst at various temperatures, and was compared with that of the free enzyme. As shown in Figure 4a, the encapsulation in silica effectively improved the thermostability of the enzyme. The effect was remarkable, particularly at higher temperatures. At 80 °C, the residual activity of the autoencapsulated CA was more than 50% after 30 min of incubation, which was much greater than that (∼10%) of the free enzyme. After 30 min at 60 °C, *ng*CA-R5@silica retained full activity while the free counterpart lost half of the initial activity. Indeed, the activity of *ng*CA-R5@silica was decreased by half only after 2.5 days of incubation at 60 °C (Figure 4b). It was also shown that the encapsulated CA exhibited 98% and 80% of its initial activity after 1 day and 5 days of incubation at 50 °C, respectively, while the residual activities of the free enzyme were 84% and 36% under the corresponding conditions (Figure 4b). In contrast, the amine-mediated biosilica lost more than 85% of its activity within 10 min at 60 °C.[3] Strong and stable silica-enzyme interactions, including the binding of R5 to silica, might be responsible for the excellent stability. Because stabilization inevitably restricts molecular flexibility,[26] which is essential to enzymatic activity, the enhanced thermostability seems to be related to the reduced catalytic performance of *ng*CA-R5@silica compared with the free enzyme.

We also investigated the effect of temperature on enzyme activity (thermoactivity) by measuring the rates of *p*-NPA hydrolysis at various temperatures (25−70 °C). When temperature was elevated, both *ng*CA-R5@silica and free enzyme showed increased activities compare to the activities at 25 °C, and a greater extent of increase was observed with the encapsulated CA (Figure 4c). The higher thermostability of *ng*CA-R5@silica compared to that of free enzyme seems to be responsible for the difference, because thermal damage on a fraction of enzyme during the experiment would result in an activity measurement lower than otherwise expected.[27] However, the difference cannot be solely attributed to the thermostability, as the catalysts showed significantly different activations even at 50 °C (Figure 4c), where they were equally thermostable (Figure 4a). The result indicates that limitation of substrate diffusion might be alleviated by thermal energy, contributing to the apparent higher activation of the encapsulated enzyme.[28] Because *ng*CA-R5@silica showed much higher normalized activities than those of free enzyme at higher temperatures (>50 °C), the estimation of the maximal activity (∼60%) of the encapsulated CA compared to free enzyme (see section 3.2) may be valid only under moderate temperature conditions (<40 °C). It is also worth noting that *ng*CA-R5@silica exhibited ∼10-fold higher activity at 60 °C compared to the activity at 25 °C (Figure 4c), while the amine-mediated biosilica showed an activity similar to that at 20 °C.[3] Considering that CO_2-capturing facilities generally operate under high temperature conditions,[6] the high thermoactivity of *ng*CA-R5@silica is a beneficial characteristic in promoting efficient CO_2 capture and sequestration. Table 2 summarizes the properties of *ng*CA-R5@silica in comparison to the amine-based biosilica, indicating the superiority of the silica nanoparticle with autoencapsulated CA.

3.4. Physical Structure of *ng*CA-R5@silica. Biosilica mediated by R5 has a spherical shape, and the diameter of a

dx.doi.org/10.1021/cs5008409 | ACS Catal. 2014, 4, 4332−4340

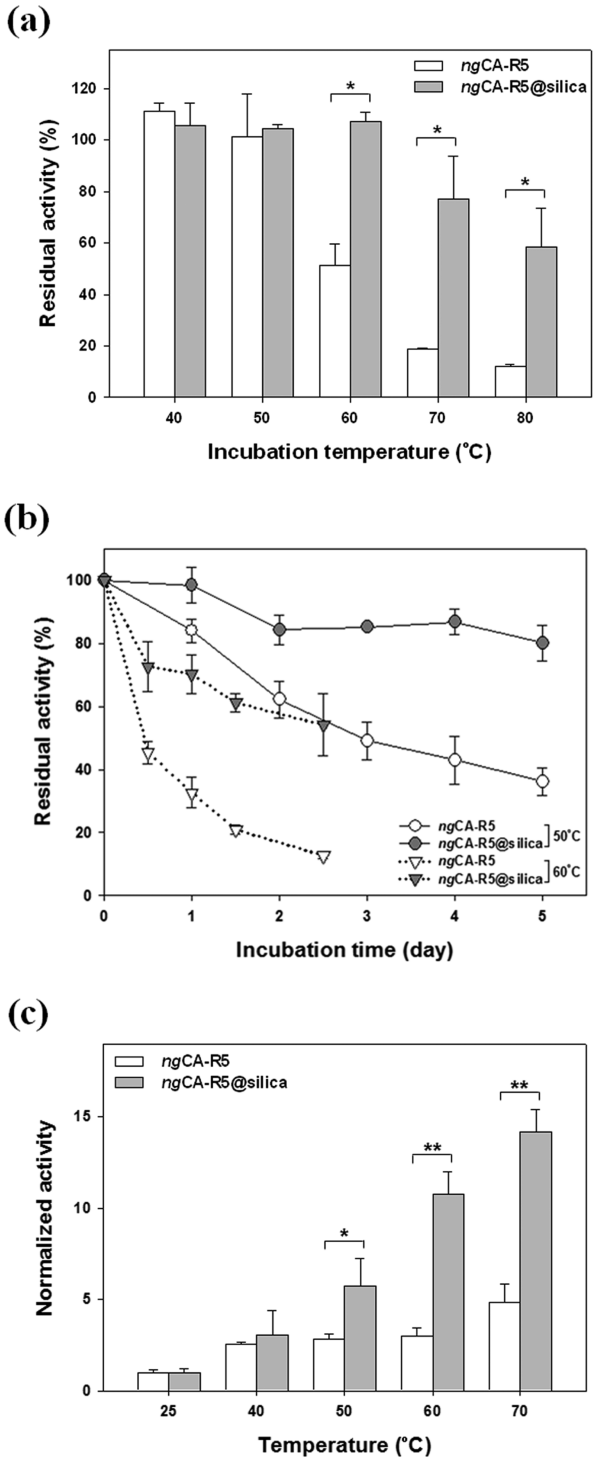

Figure 4. Thermostability and thermoactivity of *ng*CA-R5@silica. (a) Residual activities after 30 min incubation at various temperatures. (b) Long-term stability at 50 and 60 °C. (c) Effect of temperature on enzyme activity. Activities are normalized to the activity of each catalyst at 25 °C. The asterisks indicate differences with statistical significance (*p < 0.05, **p < 0.01, one-way ANOVA).

single sphere is in the range of ~300 to ~500 nm (Figure 5a), which is consistent with a previous report.[29] A closer look revealed that the surface is quite rough (Figure 5b). This feature is especially favorable in catalysis because a rough surface is expected to have a larger surface area than a smooth surface. Indeed, BET analysis estimated the surface area of

Table 2. Comparison of the Properties of the CA Encapsulation in Biosilica Matrix

	*ng*CA-R5@silica	amine-based silica
encapsulation efficiency (%)	>95%	~100%
enzyme leakage (after 24 h)	<1%	~10%
activity[a] (by esterase assay)	56%	58%
thermostability	100%[b]	<15%[c]
thermoactivity[d]	~10-fold	<1-fold
reference	this study	3

[a]Relative activity compared with activity of free enzyme, measured at 25 °C in phosphate buffer (pH 7.0). [b]Residual activity measured at 25 °C after incubation for 30 min at 60 °C. [c]Relative activity measured at 60 °C compared with activity measured at 50 °C. The amine-based silica was exposed to the high temperatures for 10 min during the measurements. It was assumed that the activity was completely retained during 10 min at 50 °C. [d]Relative activity measured at 60 °C compared with activity measured at 25 °C (*ng*CA-R5@silica) or at 20 °C (amine-based silica).

*ng*CA-R5@silica to be ~7.7 m^2/g (Table 1), which is much smaller than those of other silica materials used for enzyme immobilization[30,31] but is comparable to silica nanocomposites synthesized by bioinspired routes.[3,32,33] The pore volume and pore size were also very small (~0.002 cm^3/g and ~10 Å, respectively) (Table 1). This structural compactness seems to be another factor for promoting strong entrapment of the enzyme, but also may severely hinder inward mass transfer. Collectively, these data support the idea that the rough external surface would be relatively more important for the catalytic activity in *ng*CA-R5@silica than in others having larger surface areas (that is, higher internal pore areas). The SAED pattern indicates that the silica is amorphous as expected (Figure 5c). The particle size distribution measured by dynamic light scattering showed that most of particles are not discrete, but fused to each other, as shown in a previous study,[29] displaying an average particle size of ~2000 nm (Figure 5d). This was also evident in the TEM analysis (Figure 5b). Because surface area decreases as more particles aggregate, finding a way to control and reduce the aggregate size would improve substrate accessibility, and in turn, the catalytic performance of *ng*CA-R5@silica.

3.5. CO_2 Sequestration in $CaCO_3$ Using *ng*CA-R5@silica. Finally, the applicability of the encapsulated CA to CO_2 sequestration was examined by converting CO_2 into $CaCO_3$ using the catalyst. Because CA is known to accelerate only the rate of CO_2 hydration (subsequently, the rate of $CaCO_3$ formation), and not to affect the equilibrium of the carbonate system (that is, the final amount of $CaCO_3$ in a closed system),[34,35] we evaluated the relative rates of $CaCO_3$ formation by turbidimetric measurements.[5] When *ng*CA-R5@silica was used at 30 μg/mL on a protein content basis, the time required for the onset of $CaCO_3$ precipitation was reduced ~5.5-fold (34 s) compared with the noncatalyzed reaction (186 s) (Table 3). The initial rate of precipitation after the onset was also remarkably accelerated (Figure 6a). Notably, the biosilica exhibited ~60% CO_2 sequestration power of the free enzyme (Table 3), which coincides with the previous estimate. This may also imply that diffusive transport of HCO_3^- or CO_3^{2-} (eq 1a) out of silica matrix, which is required for the visible $CaCO_3$ precipitation, was not rate-determining. The crystal structures of the resulting precipitates formed by the different catalysts were not significantly different from each other, being mainly comprised of rhombohedral calcite with a small fraction of

dx.doi.org/10.1021/cs5008409 | ACS Catal. 2014, 4, 4332−4340

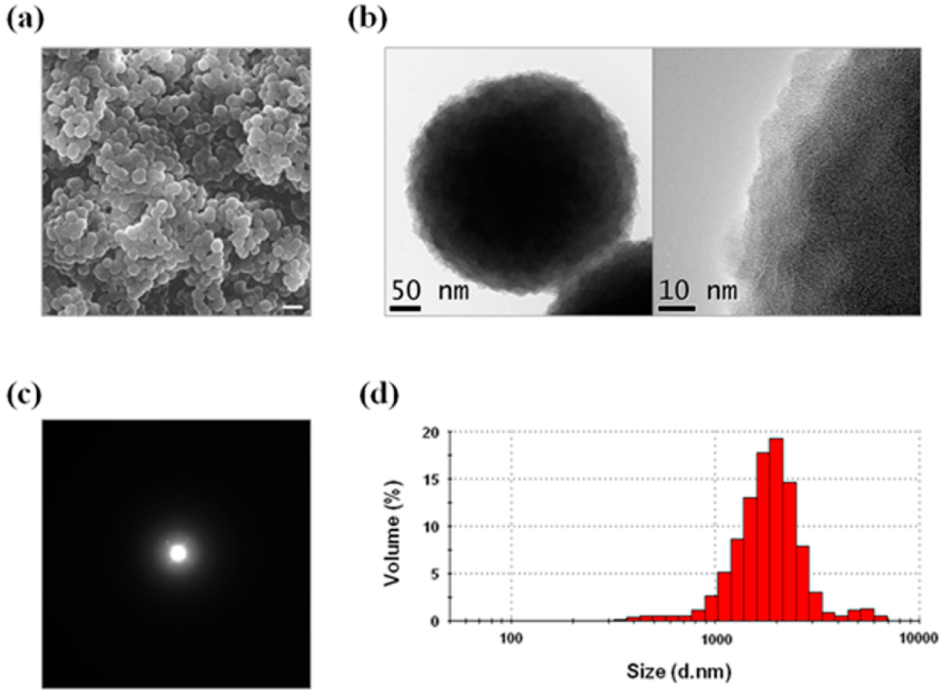

Figure 5. Structural analyses of the *ng*CA-R5@silica nanoparticle. (a) SEM image. The white scale bar at the bottom right corresponds to a length of 1 μm. (b) TEM images (left, diffraction contrast; right, high-resolution). (c) Electron diffraction pattern. (d) Size distribution of silica particles by volume.

Table 3. Time Required for the Onset of $CaCO_3$ Precipitation

			*ng*CA-R5			
sample	blank	*ng*CA-R5@silica	1.0×	0.7×	0.6×	0.5×
time (s)[a]	186 ± 9	34 ± 3	19 ± 1	28 ± 3	34 ± 2	43 ± 2

[a]Numbers are represented in mean ± SD.

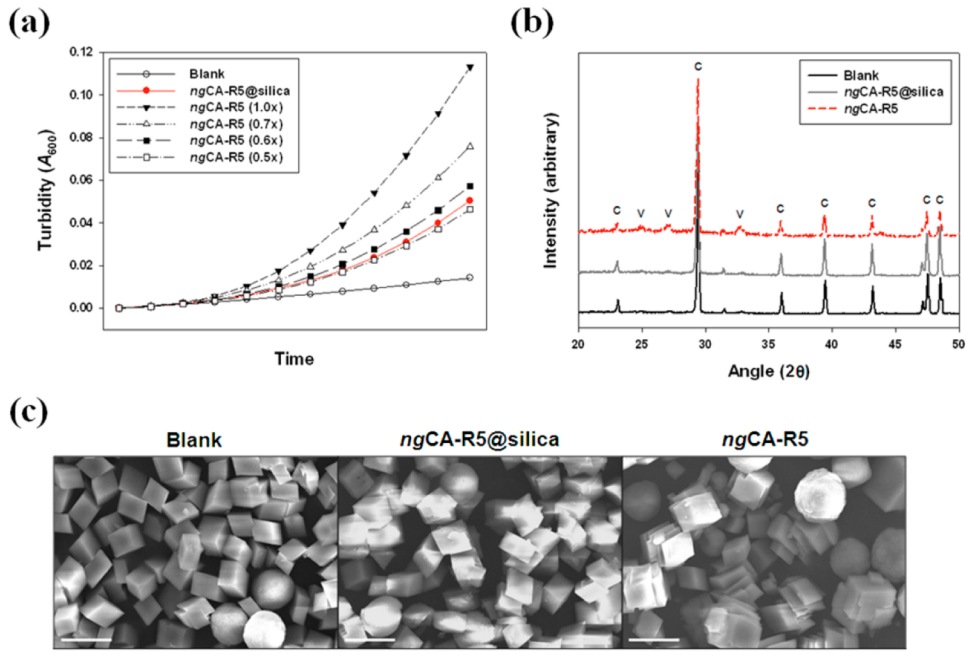

Figure 6. CO_2 sequestration in carbonate minerals using *ng*CA-R5@silica. (a) Relative initial rates of $CaCO_3$ precipitation. The curves were aligned and the turbidities were uniformly set to zero at the onset points of precipitation, facilitating comparison of the initial rate differences. (b) XRD peaks. C, calcite; V, vaterite. (c) SEM images of $CaCO_3$ powders. The white scale bar at the bottom left corresponds to a length of 10 μm.

dx.doi.org/10.1021/cs5008409 | *ACS Catal.* 2014, 4, 4332−4340

spherical vaterite (Figures 6b and 6c). The results demonstrate that the silica-CA nanocomposite can be successfully applied to CO_2 sequestration in $CaCO_3$ as an efficient accelerator without affecting the polymorphs of the resulting precipitates.

4. CONCLUSIONS

Here, we developed and characterized bioinspired silica nanoparticles with autoencapsulated recombinant *ng*CA. The autonomous silica formation, which took only a few seconds, was mediated by the silica-condensing R5 peptide fused to the *ng*CA. The encapsulation efficiency was increased as the enzyme concentration was raised. Once encapsulated, the R5-fused CA showed virtually no leakage, implying strong silica-R5 interactions. While the catalytic efficiency for esterase activity was ~53−60%, *ng*CA-R5@silica exhibited ~45% of CO_2 hydratase activity compared with the free enzyme at pH 8.5, and the efficiency was strongly pH dependent. This suggests that proton transfer is a rate limiting step for CO_2 hydration in the silica matrix. Encapsulation facilitated the reuse of the catalyst, showing 87% residual activity after reused 4 times. The thermostability of *ng*CA-R5@silica was greatly enhanced, retaining 80% of initial activity even after 5 days at 50 °C. The encapsulated CA also exhibited high thermoactivity, which is advantageous to efficient CO_2 capture. The spherical biosilica had a compact structure with a low surface area and small pore size, indicating that the outermost surface was catalytically important. The encapsulated CA successfully accelerated the rate of $CaCO_3$ formation from CO_2 with ~60% of the ability of the free enzyme, which is the expected maximal capacity of the biosilica at moderate temperatures (<40 °C). The strong and efficient interaction between silica and R5 seems to be the major factor that contributes to the excellent properties of the autoencapsulated enzyme. Collectively, the biomimetic synthesis (biosilicification) of *ng*CA-R5@silica allows this green catalyst to be efficiently applied to biomimetic CO_2 sequestration (biocalcification) with outstanding entrapment, catalytic performance, and stability.

AUTHOR INFORMATION

Corresponding Author

*Telephone: +82-54-279-2280. Fax: +82-54-279-2699. E-mail: hjcha@postech.ac.kr.

Notes

The authors declare no competing financial interest.

ACKNOWLEDGMENTS

This work was supported by the Marine Biotechnology Program (Marine BioMaterials Research Center) funded by the Ministry of Oceans and Fisheries, Korea.

REFERENCES

(1) Olajire, A. A. *Energy* **2010**, *35*, 2610−2628.
(2) D'Alessandro, D. M.; Smit, B.; Long, J. R. *Angew. Chem., Int. Ed.* **2010**, *49*, 6058−6082.
(3) Forsyth, C.; Yip, T. W.; Patwardhan, S. V. *Chem. Commun.* **2013**, *49*, 3191−3193.
(4) Barbero, R.; Carnelli, L.; Simon, A.; Kao, A.; Monforte, A. D.; Ricco, M.; Bianchi, D.; Belcher, A. *Energy Environ. Sci.* **2013**, *6*, 660−674.
(5) Jo, B. H.; Kim, I. G.; Seo, J. H.; Kang, D. G.; Cha, H. J. *Appl. Environ. Microbiol.* **2013**, *79*, 6697−6705.
(6) Savile, C. K.; Lalonde, J. J. *Curr. Opin. Biotechnol.* **2011**, *22*, 818−823.
(7) Vinoba, M.; Lim, K. S.; Lee, S. H.; Jeong, S. K.; Alagar, M. *Langmuir* **2011**, *27*, 6227−6234.
(8) Zhang, S.; Zhang, Z.; Lu, Y.; Rostam-Abadi, M.; Jones, A. *Bioresour. Technol.* **2011**, *102*, 10194−10201.
(9) Kanbar, B.; Ozdemir, E. *Biotechnol. Prog.* **2010**, *26*, 1474−1480.
(10) Wanjari, S.; Prabhu, C.; Yadav, R.; Satyanarayana, T.; Labhsetwar, N.; Rayalu, S. *Process Biochem.* **2011**, *46*, 1010−1018.
(11) Patwardhan, S. V. *Chem. Commun.* **2011**, *47*, 7567−7582.
(12) Betancor, L.; Luckarift, H. R. *Trends Biotechnol.* **2008**, *26*, 566−572.
(13) Kroger, N.; Deutzmann, R.; Sumper, M. *Science* **1999**, *286*, 1129−1132.
(14) Luckarift, H. R.; Spain, J. C.; Naik, R. R.; Stone, M. O. *Nat. Biotechnol.* **2004**, *22*, 211−213.
(15) Naik, R. R.; Tomczak, M. M.; Luckarift, H. R.; Spain, J. C.; Stone, M. O. *Chem. Commun.* **2004**, 1684−1685.
(16) Marner, W. D., 2nd; Shaikh, A. S.; Muller, S. J.; Keasling, J. D. *Biotechnol. Prog.* **2009**, *25*, 417−423.
(17) Chirica, L. C.; Elleby, B.; Jonsson, B. H.; Lindskog, S. *Eur. J. Biochem.* **1997**, *244*, 755−760.
(18) Kim, I. G.; Jo, B. H.; Kang, D. G.; Kim, C. S.; Choi, Y. S.; Cha, H. J. *Chemosphere* **2012**, *87*, 1091−1096.
(19) Elleby, B.; Sjöblom, B.; Lindskog, S. *Eur. J. Biochem.* **1999**, *262*, 516−521.
(20) Hwang, E. T.; Gang, H.; Chung, J.; Gu, M. B. *Green Chem.* **2012**, *14*, 2216−2220.
(21) Tripp, B. C.; Smith, K.; Ferry, J. G. *J. Biol. Chem.* **2001**, *276*, 48615−48618.
(22) Milligan, A. J.; Morel, F. M. M. *Science* **2002**, *297*, 1848−1850.
(23) Forsman, C.; Behravan, G.; Jonsson, B.-H.; Liang, Z.; Lindskog, S.; Ren, X.; Sandström, J.; Wallgren, K. *FEBS Lett.* **1988**, *229*, 360−362.
(24) Liang, Z.; Jonsson, B.-H.; Lindskog, S. *Biochim. Biophys. Acta* **1993**, *1203*, 142−146.
(25) Smith, K. S.; Ferry, J. G. *FEMS Microbiol. Rev.* **2000**, *24*, 335−366.
(26) Arnold, F. H.; Wintrode, P. L.; Miyazaki, K.; Gershenson, A. *Trends Biochem. Sci.* **2001**, *26*, 100−106.
(27) Carninci, P.; Nishiyama, Y.; Westover, A.; Itoh, M.; Nagaoka, S.; Sasaki, N.; Okazaki, Y.; Muramatsu, M.; Hayashizaki, Y. *Proc. Natl. Acad. Sci. U.S.A.* **1998**, *95*, 520−524.
(28) Abdel-Naby, M. A.; Sherif, A. A.; El-Tanash, A. B.; Mankarios, A. T. *J. Appl. Microbiol.* **1999**, *87*, 108−114.
(29) Knecht, M. R.; Wright, D. W. *Chem. Commun.* **2003**, 3038−3039.
(30) Wang, Y. J.; Caruso, F. *Chem. Mater.* **2005**, *17*, 953−961.
(31) Vinoba, M.; Bhagiyalakshmi, M.; Jeong, S. K.; Yoon, Y. I.; Nam, S. C. *J. Phys. Chem. C* **2011**, *115*, 20209−20216.
(32) Cardoso, M. B.; Luckarift, H. R.; Urban, V. S.; O'Neill, H.; Johnson, G. R. *Adv. Funct. Mater.* **2010**, *20*, 3031−3038.
(33) Foo, C. W. P.; Patwardhan, S. V.; Belton, D. J.; Kitchel, B.; Anastasiades, D.; Huang, J.; Naik, R. R.; Perry, C. C.; Kaplan, D. L. *Proc. Natl. Acad. Sci. U.S.A.* **2006**, *103*, 9428−9433.
(34) Uchikawa, J.; Zeebe, R. E. *Geochim. Cosmochim. Acta* **2012**, *95*, 15−34.
(35) Favre, N.; Christ, L.; Pierre, A. C. *J. Mol. Catal. B: Enzym.* **2009**, *60*, 163−170.